Journal of Solid State Chemistry **168,** 100–109 (2002)
doi:10.1006/jssc.2002.9696

Low-Temperature Phase Formation of Sn-Doped $LaMnO_{3+\delta}$ Perovskite

L. Morales,*,† A. Caneiro,*,[1] D. Vega,‡ R. Zysler,* H. Lanza,‡ and R. C. Mercader§

*CNEA-Centro Atómico Bariloche - Instituto Balseiro, S. C. de Bariloche (8400), Argentina; ‡Departamento de Física, CNEA-Centro Atómico Consitutuyentes, Argentina; §Departamento de Física, IFLP, Universidad, Nacional de La Plata, CC 67, La Plata (1900), Argentina; †CONICET, Argentina

Received January 1, 2002; in revised form April 3, 2002; accepted July 15, 2002

The incorporation of Sn into $LaMnO_3$ perovskite and its influence on magnetotransport properties were studied in samples synthesized at low temperature. Single-phase materials for two series of samples with La/(Sn + Mn) = 1 and La/(Sn + Mn) < 1 ratios were obtained by substitution of up to 10% of the Mn ions by Sn^{4+}. The effect of Sn substitution was monitored through measurements of thermal, "$M(T)$", and magnetic field, "$M(H)$", dependences of magnetization, as well as of resistivity, "$\rho(T)$", at 0 and 70 kOe. These showed that this effect depends strongly on the perovskite cation site ratio (A/B). For La/(Sn + Mn) = 1, M and T_C were depressed as Sn content was increased. The magnetization data suggest the presence of magnetic clusters with superparamagnetic behavior. No evidence of magnetoresistance (MR) was found. For La/(Sn + Mn) < 1 ratio, the samples showed ferromagnetic behavior and MR and both M and T_C raised as Sn content increased. The results are discussed in terms of A site vacancies. © 2002 Elsevier Science (USA)

Key Words: **superparamagnetism; magnetic clusters; cation vacancies; cation substitution.**

1. INTRODUCTION

The discovery of colossal magnetoresistance (CMR) in $La_{1-x}A_xMnO_3$ (A = Ca, Sr, Ba,) manganites with perovskite structure (ABO_3) has prompted in the last 5 years a very intense activity to understand the transport and magnetic properties of these materials. The CMR effect has been described by the double-exchange (DE) mechanism between Mn^{3+} and Mn^{4+} (1) and a strong electron–phonon interaction arising from the Jahn–Teller lattice distortion (2). The existence of magnetic polarons above the transition temperature (T_C) justifies the observation of the CMR at $T > T_C$ (3).

[1]To whom correspondence should be addressed. Av. Bustillo 9500, S. C. de Bariloche (8400), Rio Negro, Argentina. Fax: +54-2944-445299. E-mail: caneiro@cab.cnea.gov.ar.

Mixed Mn^{3+}/Mn^{4+} valence can be accomplished by doping the $LaMnO_3$ antiferromagnetic insulator with an alkaline-earth cation, or by self-doping increasing the oxygen content of perovskites such as $LaMnO_{3+\delta}$.

Research has recently evinced that the substitution of Mn for another ion directly modifies the magnetic ordering, especially when the latter is a transition metal (Co, Ni, Cr, Fe, Ti, etc.) because it alters the magnetic interactions in the Mn–O network. Moreover, this substitution is relevant in charge-ordered (CO) perovskites because it suppresses significantly the CO phase. Furthermore, to obtain more information about the nature of the DE coupling, the substitution of the B site of the perovskite on $Ln_{1-x}A_xMn_{1-y}B_yO_3$ materials has been studied for different cations (Al^{3+}, Ga^{3+}, Co^{3+}, Cr^{3+}, Fe^{3+}, Ti^{4+}, In^{3+}, Ge^{4+}, Sn^{4+}) (4–6). These substitutions disrupt the magnetic path between Mn^{3+} and Mn^{4+} with the consequent depression of the magnetization (5, 6).

It has also been reported that the transition temperature (T_C) from ferromagnetic metallic (FMM) to the paramagnetic insulating (PMI) state decreases as the substitution of Mn by any element increases (5, 6).

Despite all the above, only a few papers have been concerned with the incorporation of non-magnetic ions such as Sn^{4+} in the $LaMnO_{3+\delta}$ perovskite. It has been reported by some authors (7–12) that Sn incorporation in this material by synthesis at high temperatures produces a new phase with pyrochlore structure. The authors also suggested that the Sn^{4+} ion replaces La^{3+} in the resulting compound. However, we have recently indicated in a previous work (13) that the solubility of Sn^{4+} in $LaMnO_{3+\delta}$ at high temperatures is very low (< 1.00%). It seems clear that what is synthesized at high temperatures corresponds to a multiphase material composed of $LaMnO_{3+\delta}$, $La_2Sn_2O_7$, SnO_2 and Mn_3O_4 (14). On the one hand, the incorporation of Sn dopant in the samples is nearly impossible at high temperatures. Nevertheless, the solubility of Sn in the $LaMnO_{3+\delta}$ phase can be increased through the low-temperature synthesis route (13, 14). However, the

0022-4596/02 $35.00

perovskite material thus obtained is not stable at $T > 850°C$ (13). On the other hand, the results reported in the literature are not unanimous about the crystallographic site of the Sn ions or their formal valence in the Sn-doped $LaMnO_{3+\delta}$ perovskite.

In this work we prepared samples with different nominal compositions at low temperature ($T_s < 750°C$) and characterized them with different experimental techniques, in order to understand the role of Sn incorporation into the $LaMnO_{3+\delta}$ phase. We discuss the phase stability, the defect structure, the valency and occupancy of Sn in the ABO_3 structure, and the magnetic behavior of these compounds.

2. EXPERIMENTAL

Two series of samples with nominal compositions $La_{1-x}Sn_xMnO_{3+\delta}$ and $LaSn_xMn_{1-x}O_{3+\delta}$ ($x = 0$, 0.025, 0.05, 0.1, 0.15) were synthesized by the liquid-mix method (LMM) (15).

Stoichiometric proportions of La_2O_3, metallic Sn and Mn (all reactants with purity better than 99.99%) were dissolved in a diluted solution of nitric acid and dried at 200°C. The obtained nitrate was dissolved in a solution of citric acid and 2% (v/v) of ethylene glycol. The resulting material was preheated to 450°C and 600°C for 2 and 4 h, respectively, and finally treated at 725°C for 38 h. Before following this procedure, the La_2O_3 was dried at 1100°C for 12 h in order to remove absorbed or chemically bonded products such as CO_2 or H_2O.

X-ray powder diffraction data were collected on a Philips PW-1700 diffractometer using Cu$K\alpha$ radiation and a graphite monochromator. The data were obtained in the $20° \leq 2\theta \leq 80°$ range, with steps of 0.02° and counting times of 15 s per step. Structural refinements were performed using the Rietveld method (Fullprof) (16).

Samples for resistivity measurements were prepared by applying a uniaxial pressure of 1000 kg/cm^3.

High-temperature X-ray diffraction (HTXRD) studies were made on an Anton Paar HTK-10 camera coupled to the diffractometer.

^{119}Sn Mössbauer spectra were taken in transmission geometry with a nominal 5 mCi $^{119m}SnBaO_3$ source. The spectra were fitted to a Lorentzian lineshape using a non-linear least-squares program with constraints.

The homogeneity of the cation's distribution in the samples was checked by TEM-EDS analysis by means of a Philips CM200 microscope attached to an EDAX-DX4 spectrometer. The TEM was operated at 160 kV in the nanoprobe mode with a spot size of 10 nm.

The absolute oxygen contents of the samples were determined by redox titration using potassium permanganate solution (17) through the mean oxidation state of manganese ions.

D.C. magnetization (M) measurements versus temperature (T) under $H = 5$ kOe and 100 Oe and M vs magnetic field (H) at 5 K were performed with a commercial quantum design (SQUID) magnetometer. Resistivity measurements under applied magnetic fields up to 70 kOe were performed in a cryostat with a superconducting coil.

3. RESULTS AND DISCUSSION

X-ray diffraction data showed single-phase materials for x values up to 0.10 for both series of samples. For the $x = 0.15$ composition, SnO_2 was detected as a secondary phase, which indicates that the boundary of the single-phase field of the Sn-doped $LaMnO_3$ manganite is between 0.10 and 0.15. All the diffractograms reveal rhombohedral symmetry ($R\bar{3}c$).

TEM-EDS analyses were performed on several grains of the samples. The X-ray maps obtained by measuring the La$L\alpha$, Mn$K\alpha$ and Sn$L\alpha$ emission lines for $x = 0.05$ samples are plotted in Fig. 1(a) and 1(b). We have observed neither segregated Sn nor the presence of $La_2Sn_2O_7$. Therefore, the TEM-EDS analysis confirms the incorporation of Sn into the $LaMnO_3$ perovskite within a resolution of 10 nm. The variations in the gray scale may be associated with variations in the thickness of the grains.

^{119}Sn Mössbauer spectra at room temperature for $La_{0.95}Sn_{0.05}MnO_{3+\delta}$ and $LaSn_{0.05}Mn_{0.95}O_{3+\delta}$ compounds are displayed in Fig. 2(a) and 2(b), respectively. Both samples exhibit similar ^{119}Sn Mössbauer signals characteristic of Sn^{+4} with comparable isomer shifts (δ) and quadrupole splittings (Δ). In Table 1, the values of δ and Δ for the measured samples are compared with those of SnO and SnO_2 (18). Therefore, it is evident that within the experimental resolution of our spectra, Sn^{2+} is not present in our samples as previously suggested (8, 11).

The crystallographic site corresponding to the Sn^{4+} ion in the ABO_3 structure can be inferred from steric criteria and lattice symmetry. The ionic radii of Sn^{4+}, Mn^{4+} and Mn^{3+} in six-fold coordination are 0.69, 0.54, and 0.64 Å, respectively, and 1.32 Å for La^{3+} in 12-fold coordination. Therefore, taking into account the ionic radii size criteria the Sn^{4+} ion should replace Mn in the ABO_3 structure. Moreover, the coordination of Sn^{4+} is reported to be six-fold in oxide materials (19). Besides, our XRD analysis exhibits rhombohedral symmetry ($R\bar{3}c$). According to this symmetry (tilt system $a^-a^-a^-$) the A cations are nine coordinated (20), the three closest ions form a perfect trigonal planar coordination in a plane perpendicular to the three-fold axis, while the other six ions are arranged in a twisted trigonal prism around the A cations.

Both arguments exclude the presence of Sn^{4+} in the A site of the La manganites as it was recently proposed (9, 10). Therefore, taking into account the presence of Sn^{4+} in the B site of the La manganites, it is better to rewrite

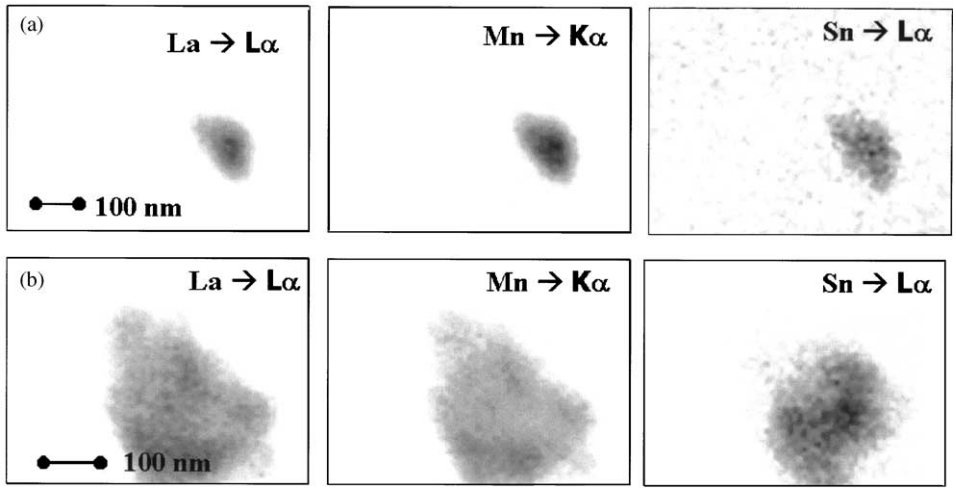

FIG. 1. (a) and (b) X-ray maps for the $La_{0.95}Sn_{0.05}MnO_{3+\delta}$ and $LaMn_{0.95}Sn_{0.05}O_{3+\delta}$ samples, respectively.

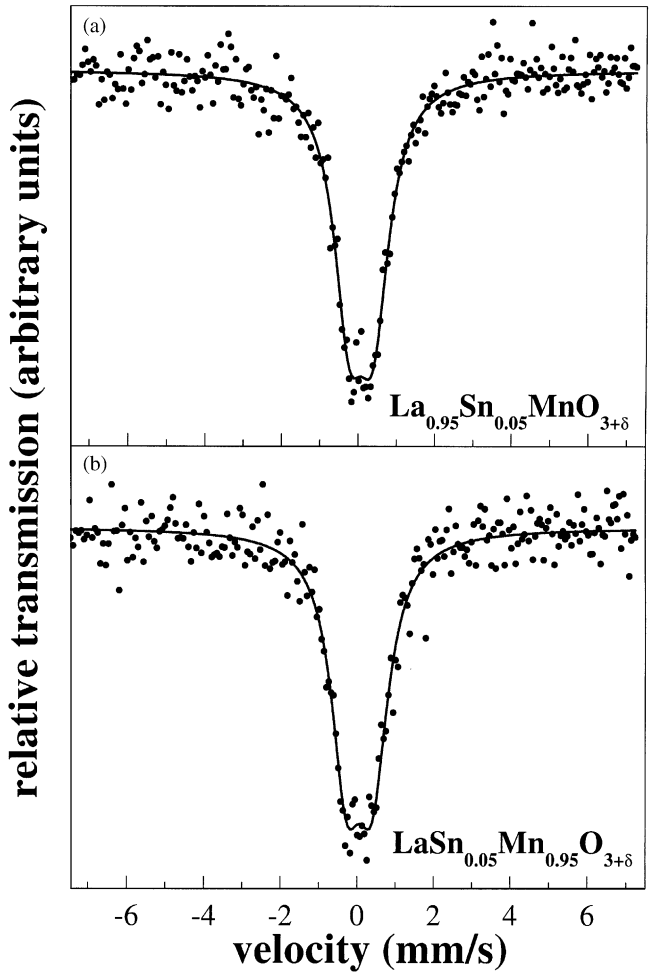

FIG. 2. (a) and (b) ^{119}Sn Mössbauer spectra for the $La_{0.95}Sn_{0.05}MnO_{3+\delta}$ and $LaMn_{0.95}Sn_{0.05}O_{3+\delta}$ samples, respectively. Solid lines are the results of the least-squares fittings described in the text.

the composition of the samples as $La_{(1-x)/(1+x)}Sn_{x/(1+x)}Mn_{1/(1+x)}O_{3+\delta}$ for the series labeled I, and $LaSn_xMn_{1-x}O_{3+\delta}$ for series II. Then, series I exhibits an A/B ratio <1 whereas for series II, $A/B = 1$.

The oxygen content values as a function of Sn concentration for both series of samples are displayed in Fig. 3. It can be observed that the oxygen content increases as Sn increases for the series with $A/B = 1$ while it decreases for the series with $A/B < 1$.

As recently reported, pure manganite cannot be oxidized higher than $\delta = 0.15$ by conventional annealing in air for samples synthesized at high temperatures (21). Nevertheless, for low-temperature synthesis, the perovskite phase can be obtained with a small grain size and with a higher concentration of Mn^{+4} (up to 42%) (22). Therefore, the higher oxygen content of our samples (series II) can be explained both by the low synthesis temperature and also by the incorporation of Sn^{4+} into the structure. For all the samples studied the measured values of oxygen content indicate the lack of oxygen vacancies in the oxygen sublattice. Thus, the point defects for the samples of series II are equal amounts of A and B site vacancies, while for series I, in addition to those produced by the extra

TABLE 1

Comparison of the Measured Mössbauer Isomer Shift (δ) and Quadrupole Splitting (Δ) Values with Those Reported for SnO and SnO_2

	$La_{0.95}Sn_{0.05}MnO_{3+z}$	$LaSn_{0.05}Mn_{0.95}O_{3+z}$	$SnO(Sn^{2+})$	$SnO_2(Sn^{4+})$
δ (mm/seg)	0.08(2)	0.06 (1)	2.6–2.8	0–0.1
Δ (mm/seg)	0.63 (3)	0.68 (3)	1.3–1.4	0.5–0.6

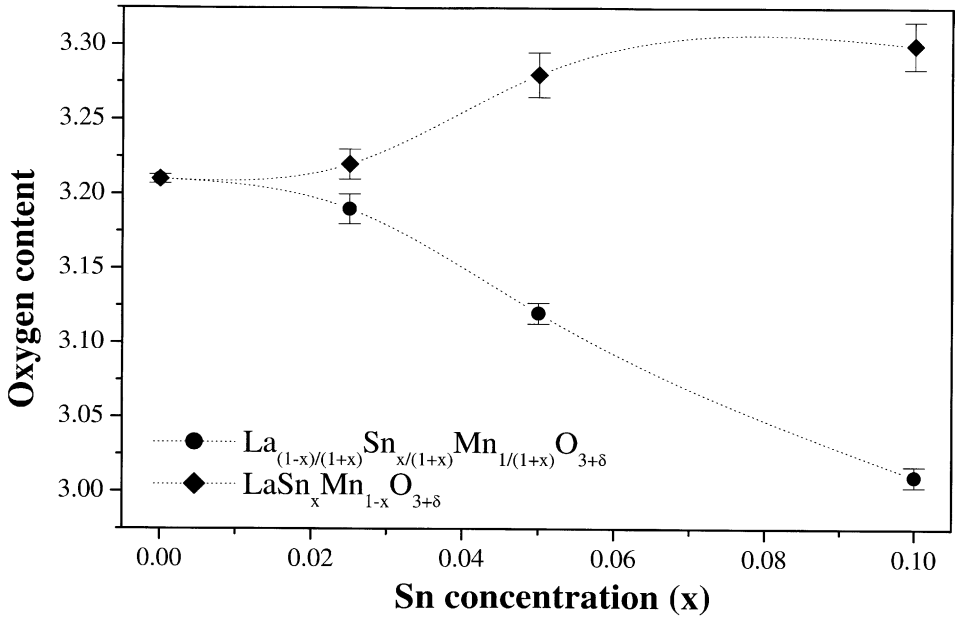

FIG. 3. Oxygen content as a function of Sn concentration for both series of samples.

oxygen we have those due to an La/(Mn + Sn) ratio lower than 1.

From the proposed $La_{(1-x)/(1+x)}Sn_{x/(1+x)}Mn_{1/(1+x)}O_{3+\delta}$ and $LaSn_xMn_{1-x}O_{3+\delta}$ formulas, we performed a refinement of the structure by the Rietveld method. In spite of the broad reflections of our data, we obtained structural parameters with satisfactory goodness of fit (R_{wp} and χ^2). However, high R_{wp} and χ^2 factors were found with a model assuming Sn as Sn^{4+} in *A* site. Fig. 4(a) and 4(b) show as an example, the Rietveld refinement for $La_{0.905}Sn_{0.048}Mn_{0.952}O_{3.12}$ and $LaMn_{0.95}Sn_{0.05}O_{3.28}$, respectively.

No significant differences were found between the lattice parameters of all samples. This result is in agreement with those reported by Töpfer *et al.* (23) for $La_{1-y}MnO_{3-(3y/2)+\delta}$ and $LaMn_{1-z}O_{3-(3z/2)+\delta}$ and Maurin *et al.* (22) for $LaMnO_{3+\delta}$. In both cases (22, 23) the percent of Mn^{4+} is higher (> 20%) and the symmetry is rhombohedral ($R\bar{3}c$). In our case the ionic radius of Sn^{4+} is similar to that of Mn^{3+}. Therefore, the comparison of the lattice parameters and unit cell volume between our results and those of Refs. (22, 23) is well grounded. A rough estimation of the Mn–O–Mn tilt angle and the Mn–O bond distances from the Rietveld refinements show a systematic variation with the increase of Sn concentration for samples of series I as we discuss below.

The stability of the Sn-doped $LaMnO_{3+\delta}$ perovskite as a function of temperature was studied by HTXRD. The XRD data at high temperature for the $La_{0.818}Sn_{0.091}Mn_{0.909}O_{3.01}$ and $LaSn_{0.1}Mn_{0.9}O_{3.30}$ are shown in Fig. 5(a) and 5(b), respectively. The temperature dependence of the diffractogram indicates that the material is stable as a single phase up to 800–810°C. At $T > 810°$ C the X-ray data show the presence of $La_2Sn_2O_7$ and SnO_2 as secondary phases for $La_{0.818}Sn_{0.091}Mn_{0.909}O_{3.01}$ and $La_2Sn_2O_7$ for $LaSn_{0.1}Mn_{0.9}O_{3.30}$.

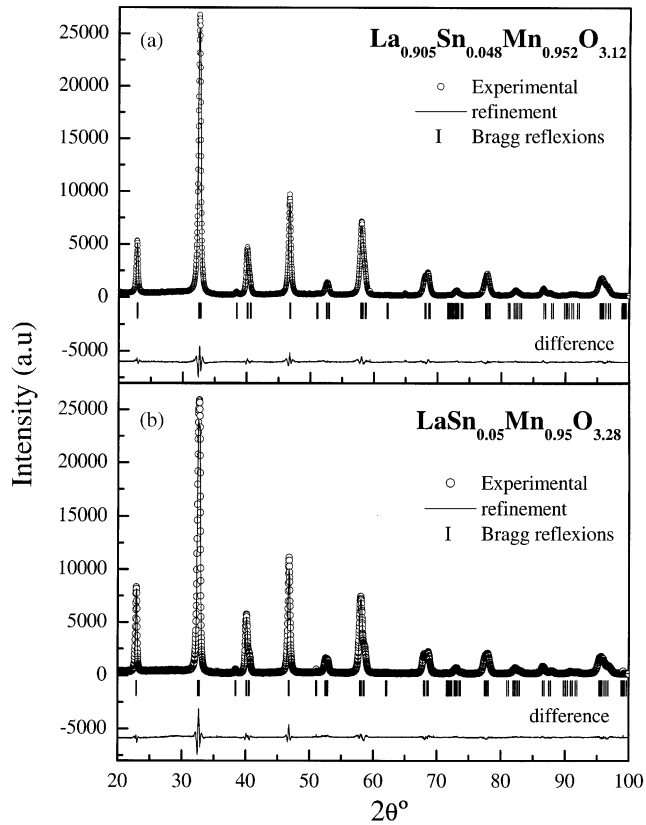

FIG. 4. (a) and (b) Rietveld refinement of $La_{0.905}Sn_{0.048}Mn_{0.952}O_{3.12}$ and $LaSn_{0.05}Mn_{0.95}O_{3.28}$, respectively.

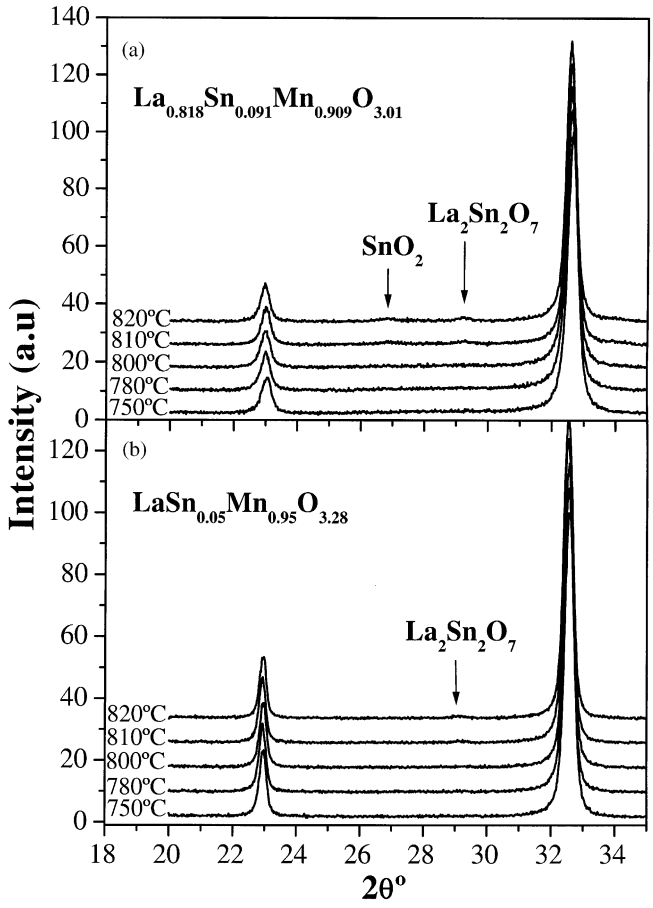

FIG. 5. (a) and (b) Powder X-ray diffraction data taken at high temperatures (HTXRD) for $La_{0.818}Sn_{0.091}Mn_{0.909}O_{3.01}$ and $LaSn_{0.05}Mn_{0.95}O_{3.28}$, respectively. The main reflections of secondary phases are indicated with arrows.

Appreciable variations of the stability temperature as a function of nominal composition have not been observed. All the samples segregate secondary phases containing Sn at $T \approx 800°C$. This suggests that the binding energy of the Sn in the ABO_3 structure is comparable for all of them.

The phase composition above the stability temperature of the Sn-doped $LaMnO_{3+\delta}$ was studied through annealing treatments at 855°C in air for periods of 12 h for all samples. Their starting compositions and the wt% of the secondary phases precipitated after heating at $T > 850°C$ are shown in Table 2. An increment of T_C and M was observed for both series of samples after the annealing treatment at $T > 850°C$. This behavior is attributed to the departure of Sn from the perovskite structure with the ensuing improvement of the double exchange interaction.

The secondary phases depend on the nominal composition as well as on the Sn content of the samples. For those with nominal compositions $LaMn_{1-x}Sn_xO_{3+\delta}$, the secondary phase corresponds to $La_2Sn_2O_7$ for all x values, while for $La_{(1-x)/(1+x)}Sn_{x/(1+x)}Mn_{1/(1+x)}O_{3+\delta}$, in addition to $La_2Sn_2O_7$, SnO_2 is present in samples with $x \geq 0.05$ (see Table 2).

TABLE 2
Wt% of Secondary Phases Formed by Heat Treatment at 855°C for Both Series of Samples

	ABO_3	$La_2Sn_2O_7$	SnO_2
$La_{0.951}Sn_{0.024}Mn_{0.976}O_{3.19}$	98	2	—
$La_{0.905}Sn_{0.048}Mn_{0.952}O_{3.12}$	96.8	2.7	0.5
$La_{0.818}Sn_{0.091}Mn_{0.909}O_{3.01}$	93	4	3
$LaSn_{0.025}Mn_{0.975}O_{3.22}$	97.8	2.2	—
$LaSn_{0.05}Mn_{0.95}O_{3.28}$	97	3	—
$LaSn_{0.1}Mn_{0.9}O_{3.30}$	94	6	—

These results can be understood considering the La:Mn ratio supported by the La manganites. Rossmalen *et al.* reported a pseudobinary La_2O_3–Mn_2O_3 phase diagram in air, where at 855°C the ABO_3 structure is stable for La:Mn ratio ranges between 0.91 and 1.20.

The departure of Sn for the $LaMn_{1-x}Sn_xO_{3+\delta}$ compounds at 855°C produces a biphasic material formed by $La_2Sn_2O_7$ and $LaMnO_{3+\delta}$ assuming that the last phase is Sn-free. According to previous results (13), the Sn content in samples heated at $T > 850°C$, if it exists, is lower than 1% at. Therefore, the final perovskite has an La:Mn ratio equal to 1.00.

The $La_{0.818}Sn_{0.091}Mn_{0.909}O_{3.01}$ sample displays an La:(Mn + Sn) ratio of 0.818, which is lower than the La:Mn = 0.908 limit given by Rossmalen *et al.* (24). Therefore, the low-temperature synthesis and the Sn incorporation increases the La poor region of the perovskite-type phase. The removal of Sn from the $La_{0.818}Sn_{0.091}Mn_{0.909}O_{3.01}$ sample at $T = 850°C$ shows $La_{1-y}MnO_3$ as the majority phase and $La_2Sn_2O_7$ and SnO_2 as minority ones.

A quantitative estimation by Rietveld analysis of the amounts of $La_2Sn_2O_7$, SnO_2 and $La_{1-y}MnO_3$ gives an La/Mn ratio closer to 0.9 which is in agreement with the La deficient limit proposed by Rossmalen (24). These data confirm the very low Sn solubility (lower than 1%) in the $LaMnO_3$ perovskite at $T > 800°C$ (13, 14). The phases obtained at $T = 850°C$ fall within the ternary La_2O_3, SnO_2, Mn_3O_4 equilibrium phase diagram.

The $M(T)$ curves obtained under an applied magnetic field of 5000 Oe for both series of samples are shown in Fig. 6(a). No appreciable differences were observed between FC (field cooling) and ZFC (zero field cooling) conditions. The $M(T)$ curve of $LaMnO_{3.21}$ falls between those corresponding to both series of samples. While in the $LaMn_{1-x}Sn_xO_{3+\delta}$ series M is depressed with Sn incorporation, in the $La_{(1-x)/(1+x)}Sn_{x/(1+x)}Mn_{1/(1+x)}O_{3+\delta}$ one, M increases as the Sn concentration increases.

The paramagnetic–ferromagnetic transition temperature T_C, evaluated from the maximal derivative of the M vs T

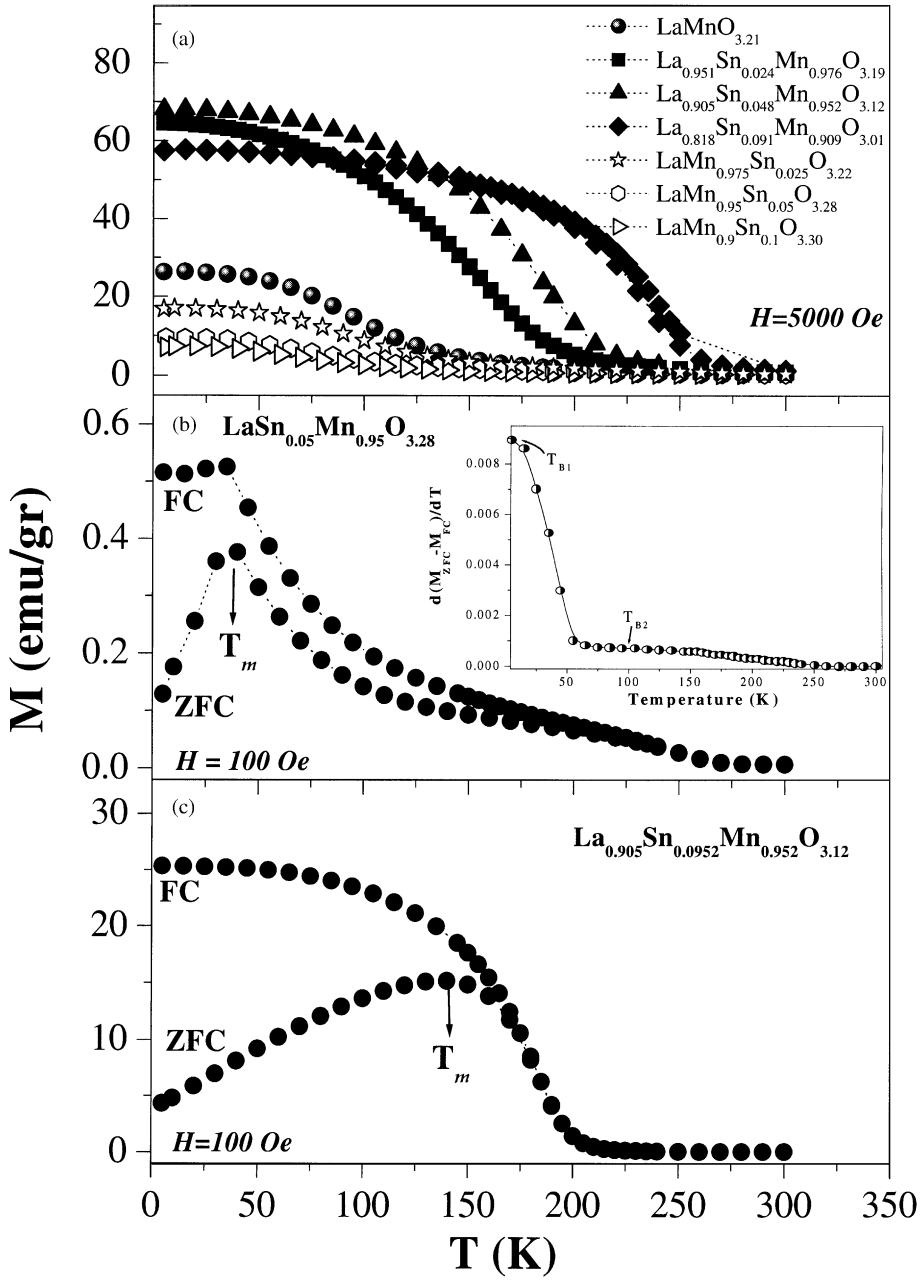

FIG. 6. (a) $M(T)$ data at 5000 Oe for $LaMnO_{3.21}$ and samples of series I and II. (b) FC and ZFC measurements at 100 Oe for $LaSn_{0.05}Mn_{0.95}O_{3.28}$ and $La_{0.905}Sn_{0.048}Mn_{0.952}O_{3.12}$, respectively. In the inset is shown the blocking temperature distribution (T_B) for $LaSn_{0.05}Mn_{0.95}O_{3.28}$.

curve at 5000 Oe, indicates that T_C should be depressed for $LaMn_{1-x}Sn_xO_{3+\delta}$ and enhanced for $La_{(1-x)/(1+x)}Sn_{x/(1+x)}Mn_{1/(1+x)}O_{3+\delta}$ samples as compared with that of $LaMnO_{3.21}$.

The FC and ZFC measurements at 100 Oe for $LaMn_{0.95}Sn_{0.05}O_{3.28}$ sample are shown in Fig 6(b). These measurements reveal clearly that T_C is around 250 K, a value much higher than that determined from the criteria of maximal derivative of the M vs T curve at 5000 Oe. Moreover, the $M(H)$ loops became linear for $T > 250$ K, confirming that T_C is around 250 K for the $LaMn_{0.95}Sn_{0.05}O_{3.28}$ sample. The same behavior is verified for all the samples of series II.

The observed difference between FC and ZFC curves reveals the progressive blocking of moments of superparamagnetic clusters, with a size distribution (distribution of relaxation times), in the presence of interparticle interactions. The ZFC magnetization, M_{ZFC}, shows a large

TABLE 3
Characteristic Values of the Magnetic Clusters for Samples of Series II

Sample	$V(cm^3)$	Φ (Å)	K (erg/cm^3)	T_B (K)
$LaSn_{0.025}Mn_{0.975}O_{3.22}$	1.96×10^{-20}	33		30
	6.81×10^{-20}	51		6
$LaSn_{0.05}Mn_{0.95}O_{3.28}$	3.94×10^{-21}	20	5.3×10^6	6
	6.09×10^{-20}	49		93
$LaSn_{0.1}Mn_{0.9}O_{3.30}$	6.19×10^{-21}	22		10

Φ represents the majority diameter of the cluster at T_B (blocking temperature), and K is the anisotropic constant.

maximum centered at a temperature T_m. Because of the presence of strong interparticle interactions, the value of T_m is not determined only by the type of particle volume distribution, as for a collection of independent blocking processes. In principle, if interparticle interactions are strong enough, they can produce a collective magnetic freezing, as for a spin glass, as reported in the literature (25–29). Actually, the maximum of M_{FC}, followed by a plateau at lower temperatures, is similar to the behavior observed in spin glasses, which are characterized by a random cooperative freezing of spins at a well-defined transition temperature at low temperatures.

The $d(M_{ZFC} - M_{FC})/dT$, which roughly indicates the blocking temperature distribution (30) for the $LaMn_{0.95}Sn_{0.05}O_{3.28}$ sample is plotted in the inset of Fig. 6(b). According to the Néel-Brown model (30, 31) for a single superparamagnetic particle the blocking temperature depends on the anisotropy energy barrier, through the Arrhenius law: $\tau = \tau_0 \exp(E_B/k_B T)$ ($E_B = KV$ for uniaxial symmetry), where E_B is the anisotropy energy barrier, K the anisotropy constant, V the particle volume, k_B the Boltzmann constant and τ_0 is the characteristic relaxation time. From FC and ZFC curves at low H (100 Oe) and $M(H)$ data, the anisotropy constant, the size of magnetic clusters and the blocking temperature have been estimated (taking a measured time $t_m = 100$ s and $\tau_0 = 10^{10}$ s) (32). The average size of the magnetic clusters varies from 40 Å for the $x = 0.025$ sample to 20 Å for that with $x = 0.10$. While the $LaMn_{0.9}Sn_{0.1}O_{3.30}$ sample exhibits only one cluster size distribution with a characteristic size of 22 Å, the other two samples show the presence of two characteristic diameters for the samples. The T_B distribution curve shows that smaller and more homogeneous clusters are formed as the Sn doping in the samples is increased. The characteristics of the magnetic clusters as a function of Sn content for samples of series II are displayed in Table 3.

The FC and ZFC curves for samples of series I show a quite different behavior. The FC and ZFC measurements for $La_{0.905}Mn_{0.952}Sn_{0.048}O_{3.12}$ are shown in Fig. 6(c). In this case, the blocking temperature of the clusters is above the ferromagnetic ordering temperature, $T_B > T_C$. Only the irreversible magnetization in the blocked regime is observed and, on increasing the temperature, the ferromagnetic order of the clusters changes to a paramagnetic state of the spins without reaching the superparamagnetic regime. The T_C values for both series of samples are shown in Table 4.

The M vs H measurements at 5 K for $LaMnO_{3.21}$, $LaMn_{0.95}Sn_{0.05}O_{3.28}$ and $La_{0.905}Mn_{0.952}Sn_{0.048}O_{3.12}$ samples are plotted in Fig. 7. These curves show the effect of Sn on the magnetic behavior of the $LaMnO_{3+\delta}$ perovskite. The $M(H)$ curve for the $LaMn_{0.95}Sn_{0.05}O_{3.28}$ sample is far from saturation. The slope of $M(H)$ at high field should correspond to the magnetic contribution of the regions between magnetic clusters. The shape of the $M(H)$ loops confirms our interpretation of the $M(T)$ curves. The $LaMn_{0.95}Sn_{0.05}O_{3.28}$ shows a typical loop originated by interacting magnetic clusters in the blocked regime ($T_B < T_C$). For $La_{0.905}Mn_{0.952}Sn_{0.048}O_{3.12}$ at $T < T_C$ all the clusters are blocked and they do not exhibit superparamagnetic behavior. The size of these clusters does allow their orientation at low field showing the typical $M(H)$ loop of a soft ferromagnet. The symmetry and the saturation of the $M(H)$ loops, shown in the inset of Fig. 7, confirm the presence of blocked magnetic clusters instead of the spin-glass-like behavior.

The resistivity curves "$\rho(T)$" under $H = 0$ and $H = 70$ kOe for $La_{0.905}Mn_{0.952}Sn_{0.048}O_{3.12}$ and $LaMn_{0.95}Sn_{0.05}O_{3.28}$ are displayed in Fig. 8(a) and 8(b), respectively. While $\rho(T)$ is sensitive to H for $La_{0.905}Mn_{0.952}Sn_{0.048}O_{3.12}$, the $LaMn_{0.95}Sn_{0.05}O_{3.28}$ one does not show any evidence of magnetoresistance (MR).

The presence of non-magnetic Sn^{4+} with a closed $3d^{10}$ shell disrupts the magnetic coupling between Mn ions. Hence, the material between magnetic clusters would be an Sn-rich magnetic insulation region exhibiting hard magnetic behavior. These regions between magnetic clusters inside each ceramic grain should be responsible for the lack of MR in the samples of series II. The electron tunneling between *FM* clusters is hampered due to the large dimensions of the Sn-intercluster regions.

TABLE 4
T_C and % Mn^{4+} (Relative to the Total Percentage of Mn) for All Samples

	T_C	$\%Mn^{4+}$
$La_{0.951}Sn_{0.024}Mn_{0.976}O_{3.19}$	159	53
$La_{0.905}Sn_{0.048}Mn_{0.952}O_{3.12}$	185	51
$La_{0.818}Sn_{0.091}Mn_{0.909}O_{3.01}$	240	51
$LaMnO_{3.21}$	95	42
$LaSn_{0.025}Mn_{0.975}O_{3.22}$	270	42
$LaSn_{0.05}Mn_{0.95}O_{3.28}$	250	54
$LaSn_{0.1}Mn_{0.9}O_{3.30}$	240	56

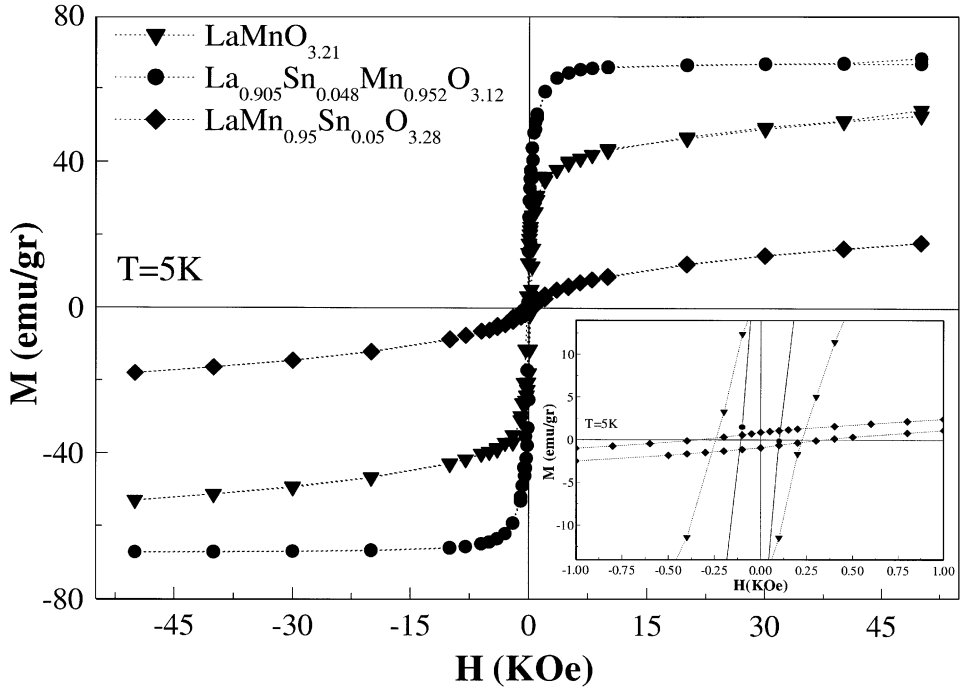

FIG. 7. $M(H)$ data at 5 K for $LaMnO_{3.21}$, $LaSn_{0.05}Mn_{0.95}O_{3.28}$ and $La_{0.905}Sn_{0.048}Mn_{0.952}O_{3.12}$.

The $La_{0.905}Mn_{0.952}Sn_{0.048}O_{3.12}$ sample shows the behavior of a soft ferromagnet where the saturation is reached at $H < 10\,000$ Oe. The magnetic clusters are close together allowing the electron tunneling process and therefore the observed MR. For these samples, T_C increases as Sn increases. This enhancement of T_C is compatible with the change of the Mn–O–Mn bond angle determined from Rietveld refinements which varies from 165° for $La_{0.951}Sn_{0.024}Mn_{0.976}O_{3.19}$ to 168° for $La_{0.818}Sn_{0.091}Mn_{0.909}O_{3.01}$. The increment of the Mn–O–Mn bond angle produces an enhancement of the strength of the ferromagnetic interactions.

Although our ceramic grains seem to be homogeneous as observed by TEM-EDS analysis, the magnetic properties of our samples are clearly heterogeneous.

The quite different magnetic behavior of both series of samples could be understood considering the A/B ratio of the samples.

In series II, the occupancies of A and B sites are equal ($A/B = 1$). The depression of M and the enhancement of T_C against $LaMnO_{3+\delta}$ is in agreement with the presence of magnetic clusters with superparamagnetic behavior. Arulraj *et al.* (33) studied the $La_{1-x}MnO_3$ and $LaMn_{1-x'}O_3$ samples for x and x' values up to 0.20. A depression of M for the $LaMn_{1-x}O_3$ series of samples and an increment of T_C and MR only for the sample with lower x value ($LaMn_{0.95}O_{3.09}$) are observed by them (33). For $A/B > 1.05$, no FM transition was observed by Arulraj *et al.* and the material becomes an insulator without evidence of MR. In the present paper, for the same La/(Mn + Sn) ratio the magnetization is depressed as compared with $LaMnO_3$ but for much lower % than that reported by Arulraj *et al.* (33). For La/(Mn + Sn) > 1.05 we are still able to observe the FM transition and the lack of MR for all Sn concentrations. It is clear that the addition of Sn to $LaMnO_3$ preserving the A/B ratio induces the formation of FM clusters with superparamagnetic behavior separated by an Sn-rich region. This Sn-rich region prevents the electron hopping between magnetic clusters with the consequent lack of MR.

In series I, the lower occupancy number of the A crystallographic site compared to that of B increases the ferromagnetic interactions between Mn ions as was reported for the La-deficient perovskite ($La_{1-x}MnO_3$) (23, 33). The effect of the A site vacancies is quite different from that produced by the B site ones. The A site vacancies are surrounded by eight Mn ions which are crystallographically and electrostatically equivalent. In this case, each La vacancy promotes the formation of three Mn^{4+} and consequently the enhancement of the DE mechanism with the surrounding Mn^{3+} forming an FM cluster. Inside these clusters, the e_g electrons are delocalized. As La vacancies are increased, the size of the ferromagnetic clusters increases (34). These clusters in the presence of a magnetic field are easily oriented lowering the magnetic barrier between them, with the consequent improvement of electron hopping and conductivity. The $\rho(H)$ vs T measurements confirm the connection between clusters in

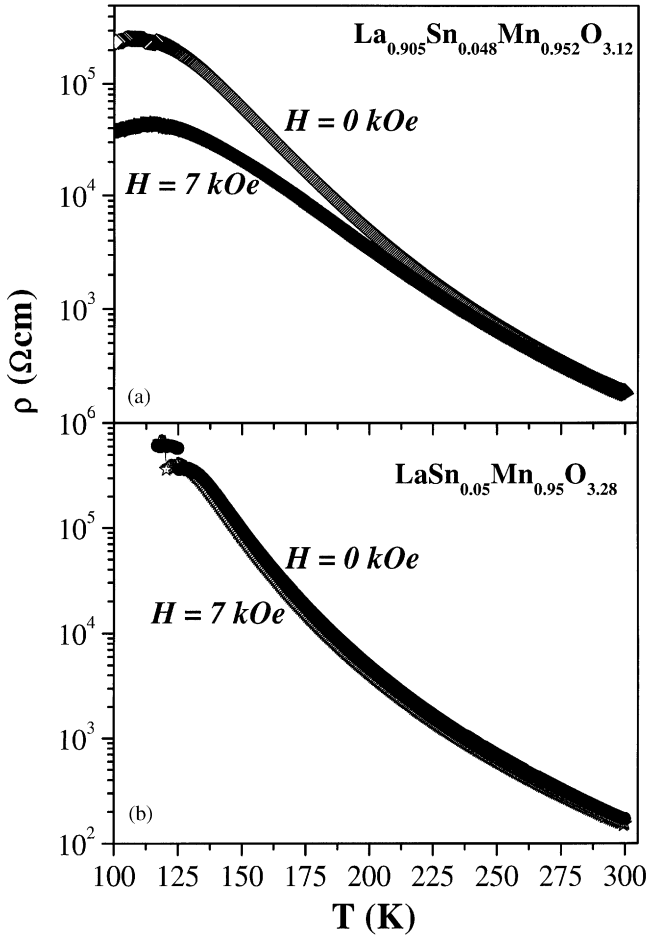

FIG. 8. (a) and (b) ρ vs T at $H = 0$ and 7 kOe for $La_{0.905}Sn_{0.048}Mn_{0.952}O_{3.12}$ and $LaSn_{0.05}Mn_{0.95}O_{3.28}$, respectively.

the presence of a magnetic field in contrast to that observed for samples of series II.

The enhancement of the FM coupling between Mn ions even at high Sn content, confirms that the effect of the A vacancies on the FM behavior is dominant over the replacement of Mn ions by Sn non-magnetic ones.

4. CONCLUSION

1. The incorporation of Sn^{4+} ions into the $LaMnO_3$ perovskite following a low-temperature synthesis route was studied for two series of samples: $LaMn_{1-x}Sn_xO_{3+\delta}$ and $La_{(1-x)/(1+x)}Sn_{x/(1+x)}Mn_{1/(1+x)}O_{3+\delta}$ ($0 \le x \le 0.10$). No Sn^{2+} ions were found in detectable amounts.

2. Each series of samples displayed a quite different magnetic behavior depending on their A/B ratio.

3. For the $LaMn_{1-x}Sn_xO_{3+\delta}$ samples the $M(T)$ and $M(H)$ measurements suggest the presence of magnetic clusters with superparamagnetic behavior. From these measurements, the characteristics of clusters were determined. From the lack of MR, it can be suggested that the regions between magnetic clusters are formed by insulator Sn-rich ones which hamper electron tunneling.

4. For the $La_{(1-x)/(1+x)}Sn_{x/(1+x)}Mn_{1/(1+x)}O_{3+\delta}$ samples, the $M(T)$ and $M(H)$ measurements indicate the presence of magnetic clusters blocked at the ferromagnetic order temperature. These clusters are easily oriented under a magnetic field showing a soft ferromagnetic behavior. Such magnetic clusters contribute to the transport due to electron hopping between thin intercluster regions.

5. In this work, the crucial role of the A/B ratio on the correct interpretation of the magnetic properties is shown. The substitution of Mn ions by non-magnetic ones can produce a very different behavior depending on the A/B ratios. Thus, an incorrect characterization of the composition of the samples can lead to a misinterpretation of the magnetotransport properties.

ACKNOWLEDGMENTS

The authors gratefully acknowledge the help of V. Grünfeld for the English revision of our manuscript. We also thank A. Esteban for the titration measurements. This work was supported by CNEA (Argentine Atomic Energy Commission), ANPCyT through PICT 99-09-05266 and CONICET (PIP-4326)

REFERENCES

1. C. Zener, *Phys. Rev.* **82,** 403 (1951).
2. A. Millis, B. I. Shraiman, and R. Mueller, *Phys. Rev. Lett.* **74,** 5144 (1995).
3. J. M. De Teresa, M. R. Ibarra, J. Blasco, J. García, C. Marquina, and P. A. Algarabel, *Phys. Rev. B* **54,** 1187 (1996).
4. B. Raveau, C. C. Martin, and A. Maignan, *J. Alloys Compd.* **275–277,** 461–467 (1998).
5. F. Damay, C. Martin, A. Maignan, and B. Raveau, *J. Magn. Magn. Mater.* **183,** 143–151 (1998).
6. B. Raveau, M. Hervieu, A. Maignan, and C. Martin, *J. Mater. Chem.* **11,** 29–36 (2001).
7. A. Sinopoulos, G. Kallias, E. Devlin, and M. Pissas, *Phys. Rev. B* **63**(1–7), 054403, (2000).
8. A. H. Morrish, Z. W. Li, S. Dai, X. Z. Zhou, J. G. Zhao, and X. M. Xiong, *Hyperfine Interact.* **113,** 485–492 (1998).
9. Z. W. Li, A. H. Morrish, and J. Z. Jiang, *Phys. Rev. B* **60**(4), 10 284–10 290 (1999).
10. Y. Q. Wang, X. F. Duan, Z. H. Wang, J. R. Sun, and B. G. Shen, *Appl. Phys. Lett.* **78**(7), 2479–2481 (2001).
11. X. Guo, Z. Chen, S. Dai, Y. Zhou, R. Li, H. Zhang, B. Shen, and H. Cheng, *J. Appl. Phys.* **88**(8), 4758–4763 (2000).
12. X. Guo, Z. Chen, D. Cui, Y. Zhou, H. Z. Huang, H. Zhang, F. Liu, K. Ibrahim, and H. Qian, *J. Cryst. Growth* **219,** 404–408 (2000).
13. L. Morales, F. Prado, A. Caneiro, R. D. Sánchez, and A. Serquis, *J. Alloys Compd.* **302**(1–2), 59–64 (2000).
14. A. Caneiro, L. Morales, F. Prado, D. G. Lamas, R. D. Sánchez, and A. Serquis, *Phys. Rev. B* **62**(10), 6825–6826 (2000).
15. A. Serquis, F. Prado, and A. Caneiro, *Physica C* **253,** 339–350 (1995).

16. Rodríguez-Carabajal, Fullprof: a program for Rietveld Refinement and Profile Matching Análisis of Complex Powder Diffraction Patterns, Laboratoire Léon Brillouin (CEA-CNRS).
17. H. L. Yakel, *Acta Crystallogr*. **8,** 394–398 (1955).
18. P. E. Lippens, J. Olivier-Fourcade, and J. C. Jumas, *Hyperfine Interact*. **126,** 137–141 (2000).
19. R. D. Shannon and C. T. Prewitt, *Acta Crystallogr. B* **25,** 925–946 (1969).
20. P. Woodward, *Acta Crystallogr. B* **53,** 44–66 (1997).
21. F. Prado, R. D. Sánchez, A. Caneiro, M. T. Causa, and M. Tovar, *J. Solid State Chem*. **146,** 418–427 (1999), doi:10.1006/jssc.1999.8386.
22. I. Maurin, P. Barboux, Y. Lassailly, J. P. Boilot, F. Villain, and P. Dordor, *J. Solid State Chem*. **160,** 123–133 (2001), doi:10.1006/jssc.2001.9204.
23. J. Töpfer and J. B. Goodenough, *Chem. Mater*. **9,** 1467–1474 (1997).
24. J. A. M. van Roosmalen, P. van Vlaanderen, E. H. P. Cordfunke, and W. L. Ijdo, *J. Solid State Chem*. **114,** 516–523 (1995), doi:10.1006/jssc.1995.1078.
25. T. Jonsson, P. Svedlindh, and M. F. Hansen, *Phys. Rev. Lett*. **81,** 3976 (1998).
26. J. L. Dormann, R. Cherkaoui, L. Spinu, M. Nogues, F. Lucari, F. D'Orazio, D. Fiorani, A. Garcia, E. Tronc, and J. P. Jolivet, *J. Magn. Magn. Mater*. **187,** L139 (1998).
27. E. Tronc, A. Ezzir, R. Cherkaoui, C. Chaneac, M. Nogues, H. Kachkachi, D. Fiorani, A. M. Testa, J.M. Greneche, and J. P. Jolivet, *J. Magn. Magn. Mater*. **221,** 63 (2000).
28. R. D. Zysler, C. A. Ramos, E. De Biasi, H. Romero, A. Ortega, and D. Fiorani, *J. Magn. Magn. Mater*. **221,** 37 (2000).
29. R. D. Zysler, D. Fiorani, and A. M. Testa, *J. Magn. Magn. Mater*. **224,** 5 (2001).
30. J. L. Dormann, D. Fiorani, and E. Tronc, in "Magnetic Relaxion in Fine Particle Systems" (I. Prigogine and S.A. Rice, Eds.), Advance in Chemical Physics, Vol. XCVIII, John Wiley & Sons, Inc, New York, (1997).
31. L. Néel, *J. Phys. Soc. Japan* **17**(Suppl. B1), 676 (1961).
32. L. Morales, A. Caneiro, R. D. Sánchez, and D. Vega, *J. Magn. Magn. Mater*. **226–230,** 823 (2001).
33. A. Arulraj, R. Mahesh, G. N. Subbanna, R. Mahendiran, A. K. Raychaudhuri, and C. Rao, *J. Solid State Chem*. **127,** 87–91 (1996), doi:10.1006/jssc.1996.0360.
34. M. Muroi and R. Street, *Aust. J. Phys*. **52,** 205 (1999).